water

Article

Study on the 3D Hydrodynamic Characteristics and Velocity Uniformity of a Gravity Flow Circular Flume

Yi Zhang [1,2], Longxi Han [1,2,*], Lina Chen [1,3], Chenfang Wang [1,2], Bo Chen [1,2] and Anqi Jiang [1,2]

1 Key Laboratory of Integrated Regulation and Resource Development on Shallow Lake of Ministry of Education, College of Environment, Hohai University, Nanjing 210098, China; hhuzhangyi@126.com (Y.Z.); chenlina2001@163.com (L.C.); wangchenfang0316@163.com (C.W.); grchb@163.com (B.C.); zaizai123202103@163.com (A.J.)
2 College of Environment, Hohai University, Nanjing 210098, China
3 College of Agricultural Science and Engineering, Hohai University, Nanjing 210098, China
* Correspondence: hanlongxi@sina.com

Abstract: Flumes have been widely used in water conservancy science and environmental science research. It is of great significance to obtain the hydrodynamic characteristics and flow field uniformity in the flume. In this study, a new type of annular flume was taken as an example. The 3D flow field was simulated by using a commercial computational fluid dynamics (CFD) code, and was also measured by acoustic doppler velocimeter (ADV) to verify the simulation results. The average relative error range was between 8.37% and 9.95%, the simulated results basically reflected the actual situation of the flow field. On this basis, the structural characteristics of flow field were analyzed. A new calculation method of flow velocity uniformity was presented according to the flow characteristics of natural open channels. The velocity uniformity in the straight channel was calculated and analyzed based on this method, and the influence of speed on the velocity uniformity was further discussed. The length of uniform section was negatively correlated with the rotational speed (average velocity), which was between 39 cm and 101 cm in the straight, and the uniformity coefficient was less than 10%. Finally, the water flow characteristics in the straight channel without wheel were compared with the natural open channel flow. The longitudinal velocity was well fitted with the Prandtl logarithmic distribution formula ($R^2 > 0.977$), and the application feasibility of the flume was analyzed. This study can provide technical support for the development and application of annular flume.

Keywords: annular flume; CFD; gravity flow; hydrodynamic characteristics; velocity distribution uniformity

check for updates

Citation: Zhang, Y.; Han, L.; Chen, L.; Wang, C.; Chen, B.; Jiang, A. Study on the 3D Hydrodynamic Characteristics and Velocity Uniformity of a Gravity Flow Circular Flume. *Water* **2021**, *13*, 927. https://doi.org/10.3390/w13070927

Academic Editor: Helena M. Ramos

Received: 24 February 2021
Accepted: 17 March 2021
Published: 29 March 2021

Publisher's Note: MDPI stays neutral with regard to jurisdictional claims in published maps and institutional affiliations.

Copyright: © 2021 by the authors. Licensee MDPI, Basel, Switzerland. This article is an open access article distributed under the terms and conditions of the Creative Commons Attribution (CC BY) license (https://creativecommons.org/licenses/by/4.0/).

1. Introduction

Annular flume has been widely used in water conservancy science and environmental science research because of its covering a small area, and there being no water backflow device or influence of inflow and outflow. The hydrodynamic characteristics of different annular flumes are different due to the differences in shape and driving mode. Hydrodynamic forces directly affect the release, migration and diffusion of pollutants and sediment in water. Therefore, it is of great significance to design different annular flumes that accord with the hydrodynamic characteristics of different natural water bodies, and to obtain the hydrodynamic characteristics and flow field uniformity in the flumes.

The shape of existing annular flumes is mainly circular or runway. The main driving modes of water flow in the flumes include water surface drive or sidewall drive. More specifically, the water flow is driven by a moving cover located on the water surface [1], a wheel that is at a tangent to the water surface [2], or a surface wind from a blower [3]. In another design, the water flow is driven by the rotation of the inner and outer groove walls [4]. The natural state waters can be roughly divided into three types according to their hydrodynamic characteristics, including the gravity runoff type in rivers, the wind-driven circulation type in lakes or reservoirs, and the tidal type in estuaries and bays [5]. These existing annular flumes do not adequately meet the experimental needs for simulating gravity flow. In previous studies, most of the annular flumes simulated the wind-driven flow with the driving devices located on the water surface [2,6,7]. The gravity flow [8–11] and wave [12–14] simulation devices were predominantly straight flumes, covering a large area. Thus, it can be seen that no annular flume has been published or put into practical use that can simulate the gravity flow of natural rivers. Furthermore, understanding of the hydrodynamics of these kinds of devices is lacking.

In addition, the uniformity of velocity distribution in the flume will directly affect the accuracy of quantitative relationship establishment in the experiment. Mastering the flow structure and velocity distribution uniformity in the flumes is also one of the necessary conditions for carrying out hydrodynamics experiments. In previous experiments with annular flume, the average value of hydrodynamic parameters in the experiment was usually represented by the hydrodynamic characteristic values in the middle of a straight channel [2,15]. The influence of curve flow was usually ignored. There is a lack of quantitative analysis of the influence of the curve and the uniformity of the flow velocity on the section.

In this study, a new type of bottom-driven annular flume (patent no.: ZL201711059444.2) that can simulate the characteristics of natural gravity flow was taken as the research object. A 3D mathematical model was established by using the commercial computational fluid dynamics (CFD) code Fluent software package to simulate its hydrodynamic characteristics. An Acoustic Doppler Velocimeter (ADV) was used to measure the 3D water flow characteristics and the accuracy of the mathematical model was further verified. Different typical profiles were cut, and the distribution characteristics of the 3D flow field were analyzed on the basis of the established mathematical model. Because of the uneven distribution of longitudinal velocity in vertical direction of the natural gravity flow, the existing method for calculating the uniformity coefficient was improved, thus presenting a new method for calculating the comprehensive uniformity coefficient of natural water. This method was used to calculate the distribution of the velocity uniformity coefficient in the straight section of the flume and to quantify the uniformity index. Finally, the effect of rotational speed on velocity uniformity was studied. This study can provide technical support for the research and development of different types of flume, exploration of water flow structure and analysis of flow velocity uniformity. In addition, it can be used in related scientific research fields such as sediment, pollutant release, migration and diffusion.

2. Models and Methods

2.1. Physical Model

The main structure of the experimental flume is a racetrack-shaped circular trench (see Figure 1A,C). The straight path is 1.5 m long, and the inside and outside diameters of the curves at both ends of the flume are 0.4 m and 1 m. The wheel, which has a diameter of 0.25 m, is located at the bottom of the beginning of the straight path. The experimental water depth was set at 0.3 m. The working principle of the flume is to generate shear force by driving the wheel with an adjustable motor. The wheel drives the water flow in the flume, so as to realize the increase of flow velocity from the bottom to the surface in a vertical direction (see Figure 1B).

2.2. Experimental Test

Considering the influence of the wheel, we did not carry out related flow rate research and verification work in Straight I and Curve II. Four sections were arranged, including one for Curve I (S1) and three for Straight II (S2–S4). Five perpendicular lines were set for each section (V1–V5). The setting of the measuring points on each vertical line was as follows: the distance between each pair of measuring points was 0.5 cm between 0 and 5 cm above the bottom, which was 1 cm between 5 and 15 cm and 2 cm between 15 and

30 cm. The setting of the measured section, perpendicular lines and measuring point is shown in Figure 1C,D.

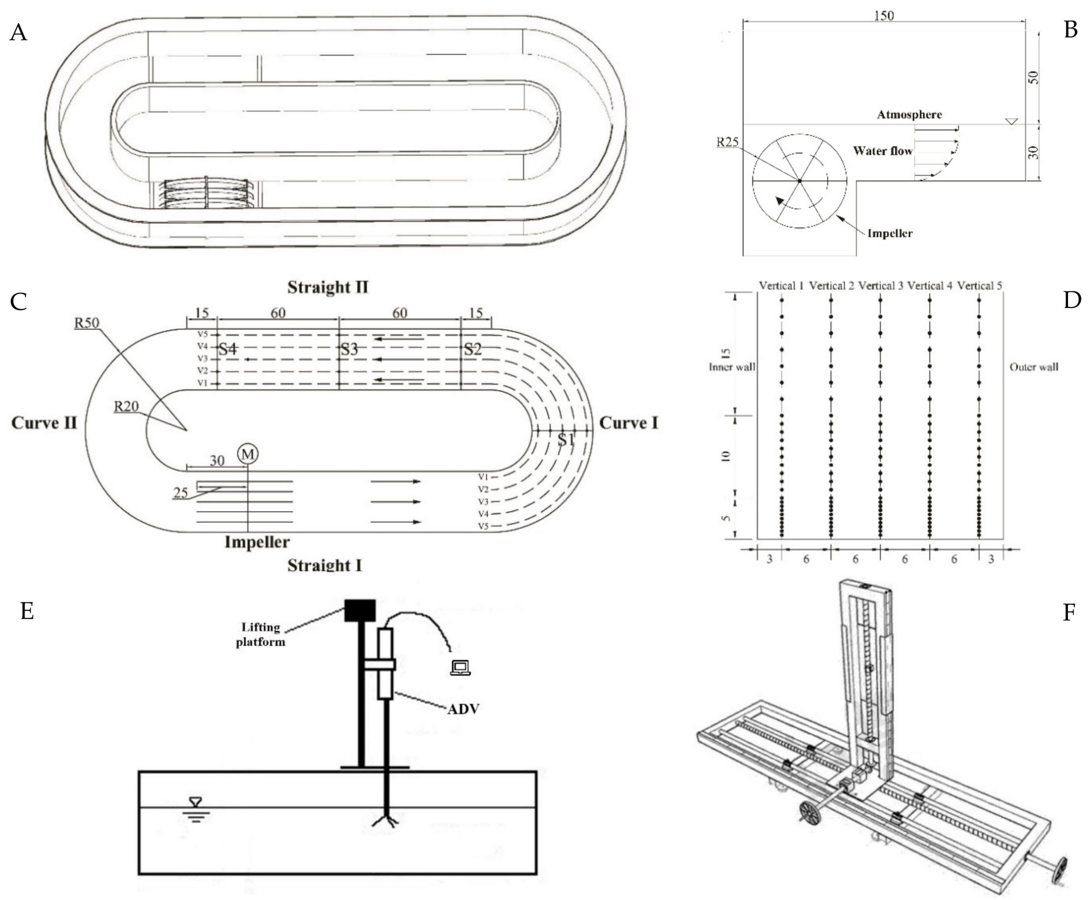

Figure 1. Schematic diagram of circular flume and arrangement of measuring points. (**A**) Generalization of physical model of flume, (**B**) working schematic, (**C**) layout of measuring section and vertical line, (**D**) arrangement of measuring points on each vertical line, (**E**) schematics of the velocity measurement system, (**F**) schematics of the lifting platform.

The three-dimensional velocity component of each measurement point was measured by the velocity measurement system, including an Acoustic Doppler Velocimeter (ADV), lifting platform and vertical scale. The ADV (operating frequency of 10 MHz, see Figure 1E) was produced by the SonTek company (San Diego, CA, USA), with a resolution of 0.01 cm/s and a sampling frequency range of 0.1 to 25 Hz (10 Hz was used in this experiment). The schematics of the velocity measurement system are shown in Figure 1E and the schematics of the lifting platform are shown in Figure 1F. We mounted the device between the inner and outer walls of the flume, fixed the ADV, and tested the hydrodynamic parameters at different points by adjusting the position of the screw rod, the distance of which was provided by the vertical scale. The longitudinal, transverse and vertical flow rates are expressed as U, V and W, respectively, where the longitudinal velocity U was positive in the counterclockwise direction, the transverse velocity V was positive in the inner wall to the outer wall, and the vertical velocity W was positive in the upward direction.

2.3. Mathematical Model

The annular flume has strong three-dimensional flow motion characteristics. The American CFD commercial software Fluent (the version number was 19.2), which is popular in the world at present, was used to establish a three-dimensional flow model to simulate its hydrodynamic characteristics. The k-ε turbulence model of RNG was used, and the governing equations are as follows:

1. Continuity equation:

$$\frac{\partial \rho}{\partial t} + \frac{\partial \rho u_i}{\partial x_i} = 0 \tag{1}$$

2. Momentum equation:

$$\frac{\partial \rho u_i}{\partial t} + \frac{\partial}{\partial x_j}(\rho u_i u_j) = -\frac{\partial p}{\partial x_j} + \frac{\partial}{\partial x_j}\left[(\mu + \mu_t)\left(\frac{\partial u_i}{\partial x_j} + \frac{\partial u_j}{\partial x_i}\right)\right] \tag{2}$$

3. k-ε equation:

$$\frac{\partial(\rho k)}{\partial t} + \frac{\partial(\rho k u_i)}{\partial x_i} = \frac{\partial}{\partial x_j}\left[\alpha_k(\mu + \mu_t)\frac{\partial k}{\partial x_j}\right] + G_k - \rho\varepsilon \tag{3}$$

$$\frac{\partial(\rho \varepsilon)}{\partial t} + \frac{\partial(\rho \varepsilon u_i)}{\partial x_i} = \frac{\partial}{\partial x_j}\left[\alpha_\varepsilon(\mu + \mu_t)\frac{\partial \varepsilon}{\partial x_j}\right] + C_{1\varepsilon}^* \frac{\varepsilon}{k} G_k - C_{2\varepsilon}\rho\frac{\varepsilon^2}{k} \tag{4}$$

$$G_k = \mu_t\left(\frac{\partial u_i}{\partial x_j} + \frac{\partial u_j}{\partial x_i}\right)\frac{\partial u_i}{\partial x_j} \tag{5}$$

$$\mu_t = \rho C_u \frac{k^2}{\varepsilon} \tag{6}$$

$$C_{1\varepsilon}^* = C_{1\varepsilon} - \frac{\eta(1 - \eta/\eta_0)}{1 + \beta\eta^3} \tag{7}$$

where ρ—density of the fluid, t—time, u_i, u_j—velocity component, x_i, x_j—coordinate component, p—fixed pressure, μ—kinematic viscosity coefficient, μ_t—turbulent viscosity coefficient, G_k—turbulent kinetic energy, and C_u = 0.0845, $\alpha_k = \alpha_\varepsilon = 1.39$, $C_{1_\varepsilon} = 1.42$, $C_{2\varepsilon} = 1.68, \eta_0 = 4.377, \beta = 0.012$.

2.4. Generalized Model

According to the physical model shown in Figure 1A, the software Gambit (the version number was 2.4.6) was used for modeling at a proportion of 1:1. For convenience of expression, the model was divided into Straight I, Curve I, Straight II, Curve II and the wheel area. An overall generalization of the model is shown in Figure 2A, and the generalization of the wheel area is shown in Figure 2B.

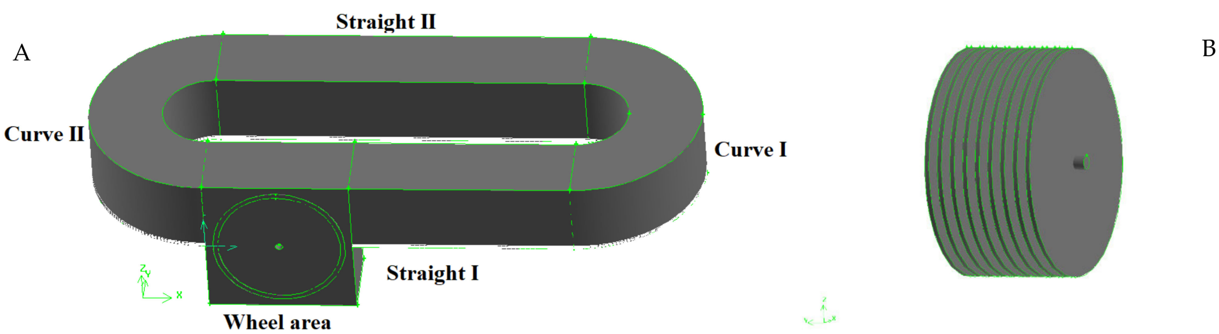

Figure 2. Flume model establishment and partition. (**A**) Overall generalization of the model, (**B**) generalization of the wheel area.

2.5. Mesh Generation

The flume grid was composed of tetrahedral unstructured grids. The interval size was 0.02 m in Straight I and II, 0.015 m in Curve I and II, and 0.01 m in the wheel area. To give due consideration to calculation accuracy and speed, the mesh near the wall was encrypted. The total grid division number of the overall model was 1,070,393, and the grid division diagram is shown in Figure 3.

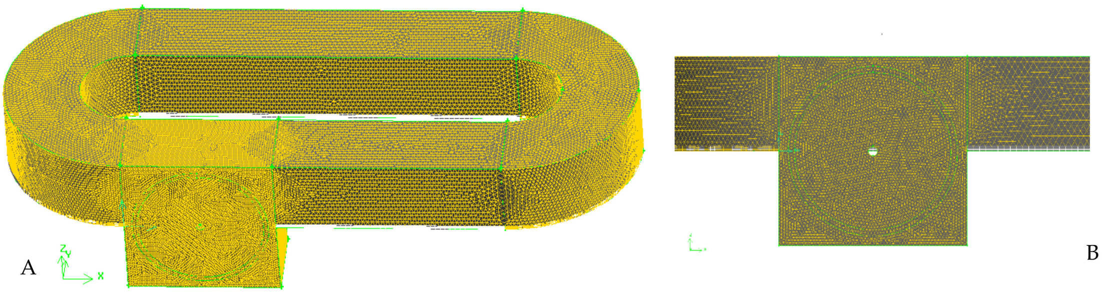

Figure 3. The grid division of the flume model and the details of the wheel position. (**A**) Global grid diagram, (**B**) grid diagram of the wheel area.

2.6. Boundary Conditions

The mathematical model did not involve the boundary conditions of the inlet and outlet. The conditions of the water surface and the wall surface were set as follows.

Free surface: the most commonly used methods in research include the rigid-lid hypothesis method and the volume of fluid (VOF) method. The VOF method has disadvantages such as complex and time-consuming calculation. The free surface was set as being symmetrical in this research to simplify the calculation.

Drive wheel: the wheel was the only source of power for the water flow in the flume and was set as a moving wall during the simulation. On the direct contact surface between the moving grid and the fixed grid, the two surfaces were combined into one interface by setting it as the "interface", which was used as the source of fluid power in the flume. After many numerical model trial calculation tests, the mesh was iterated so that the average value of the parameter y+ was 32.5, the wall roughness height (Ks) was determined to be 0.001 cm, and the roughness constant (Cs) was set to 0.5.

Wall and bottom: the bottom and the side of the flume were always stationary. They were set as a non-sliding wall surface, and the standard wall function was used to modify it.

2.7. Model Selection and Solution Method

The multiple reference frame (MRF) model was adopted to simulate the wheel area. The finite volume method was used to solve the mass conservation equation and Navier-Stokes equation. The k-ε turbulence model of RNG was used, which can simulate transient flow and streamline bending better than the standard k-ε model [16,17]. The simulation was transient, and PISO was used for coupling calculation of pressure and velocity fields. At the same time, the influence of gravity was considered, with the acceleration of gravity being taken as 9.81 m/s^2. If the residual of each variable was lower than 0.001 or the residual was basically unchanged with iteration, the calculation can be considered to be convergent.

2.8. Calculation Method of Velocity Uniformity Index

Research on velocity distribution uniformity has seldom been performed in traditional hydraulics and river dynamics. It has been studied and applied to SCR reactors, automobile three-way catalytic converters, desulfurization spray towers, and in many other industrial fields. However, there is no uniform uniformity calculation method or corresponding evaluation index. Existing calculation methods include the relative standard deviation method [18], the uniformity of Weltens establish index [19], the weighted average flow velocity uniformity index method based on the area or quality [20], the Christiansen uniformity coefficient method [21], and the number of DU method [22].

However, the natural gravity flow in this paper has the characteristics of three-dimensional velocity distribution. The longitudinal velocity is distributed unevenly in the vertical direction, and is generally thought of as being a logarithmic or exponential distribution. As a result, it is impossible to judge the uniformity simply by referring to the previous uniformity calculation methods. A new method to determine the comprehensive uniformity coefficient of a section is proposed in order to calculate the uniformity of the flow velocity of natural gravity flow. The specific calculation method is as follows:

(1) Stratify a cross-section horizontally (I = 1, 2, 3, . . . , n). The number of layers and the location distribution of each layer can be set according to specific needs. In this paper, three layers may be set, which are 2 cm, 15 cm and 28 cm from the bottom.

(2) The uniformity coefficients of each layer in all directions were calculated in turn using the relative standard deviation method.

$$\gamma_{i,x} = \frac{S_{i,x}}{\overline{v_{i,x}}} \times 100\% \tag{8}$$

$$S_{i,x} = \sqrt{\frac{1}{n-1}\sum_{j=1}^{n}\left(v_{i,j,x} - \overline{v_{i,x}}\right)^2} \tag{9}$$

where $\gamma_{i,x}$—the uniformity coefficient of each layer in the X direction, $v_{i,j,x}$—velocity in the X direction of each measurement point, $\overline{v_{i,x}}$—the average velocity in the X direction of layer i. (The uniformity coefficients in the Y and Z directions were calculated in the same way).

(3) Set the weight of the flow velocity in three directions. The weight ratio of the flow velocity in each direction was consistent with the ratio of the average flow velocity. Then the uniformity coefficients of each layer were calculated.

$$\beta_x : \beta_y : \beta_z = \overline{v_{i,x}} : \overline{v_{i,y}} : \overline{v_{i,z}} \tag{10}$$

$$\beta_x + \beta_y + \beta_z = 1 \tag{11}$$

$$\gamma_i = \beta_x\gamma_{i,x} + \beta_y\gamma_{i,y} + \beta_z\gamma_{i,z} \tag{12}$$

where γ_i—comprehensive uniformity coefficient of each layer, β_x, β_y, β_z—the weight of flow velocity in the x, y, and z directions.

(4) Set the weight of each layer according to the actual needs. If the surface release of light water pollutants such as oil is being studied, the surface weight can be increased. When studying sediment bed surface release, the bottom weight can be increased.

$$\sum_{i=1}^{n}\alpha_i = 1 \tag{13}$$

where α_i—the weight of each layer. In this paper, the influence of different layers was not considered, that is, the weights of each layer were equal.

(5) The weighted average value of the uniformity coefficients of each layer and direction was calculated. The value was the comprehensive uniformity coefficient of the section, which can be used as the evaluation standard for the uniformity of flow velocity in the section.

$$\gamma = \frac{1}{n}\sum_{i=1}^{n}\alpha_i\gamma_i \tag{14}$$

where γ—comprehensive uniformity coefficient of section. The uniformity is better when the value is smaller.

3. Results and Discussion

3.1. Simulation Results and Verification

Section S1 (see Figure 1C) of curve I and section S2–S4 of straight II were selected for verification analysis. The locations of the sections are shown in Figure 1C. The positive direction of the 3D flow velocity simulation values was adjusted to be the same as the positive direction of the ADV test results. According to the simulated and measured results, the data of five lines in each cross-section were plotted in the same figure. When the longitudinal and transverse velocity was plotted, the *X*-axis was the flow rate, and the

Y-axis was the height from the bottom of the flume. To make the figure beautiful and clear, the longitudinal velocity of vertical line V2~5 was increased by 10 units for drawing, and the transverse velocity of vertical line V1~5 was increased by 5 units for drawing. When the vertical velocity was plotted, the *X*-axis was L/B (L was the distance from the measuring point to the inner wall, and B was the trench width, taken as 30 cm), and the *Y*-axis was the velocity.

The verification results are shown in Figure 4 and the relative error results are shown in Table 1. In section S1 of curve I, the simulated results were basically the same as the measured results, and the data were in good agreement. The average relative error range of all vertical velocity measured by current measurement was between 8.37% and 9.95%, and the maximum relative error was between 14.83% and 19.96%. In section S2–S4 of straight II, the simulated results were in good agreement with the measured results, especially at 5–20 cm from the bottom of the flume. The deviation of the bottom area and the near surface area was slightly larger, but the flow characteristics and trend were basically the same. The relative error ranges of longitudinal velocity for all of the vertical measured lines in section S2–S4 were between 4.81–7.49%, 4.98–7.10% and 5.67–7.79%, and the maximum relative error ranges were between 9.54–13.93%, 13.84–14.33% and 13.94–21.43%. The simulated velocity distribution basically reflected the actual situation of the flow field in the flume, and the numerical simulation results were generally satisfactory.

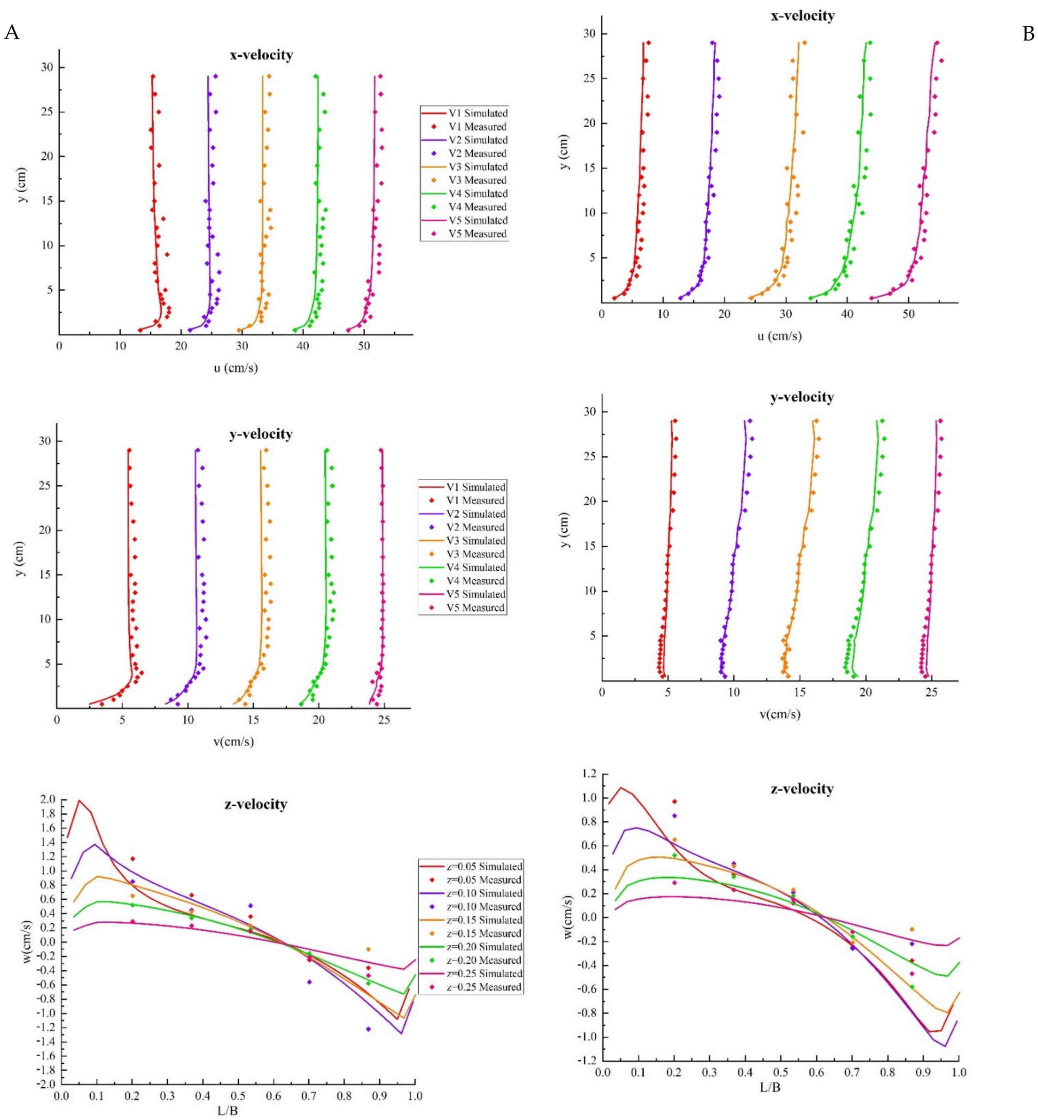

Figure 4. *Cont.*

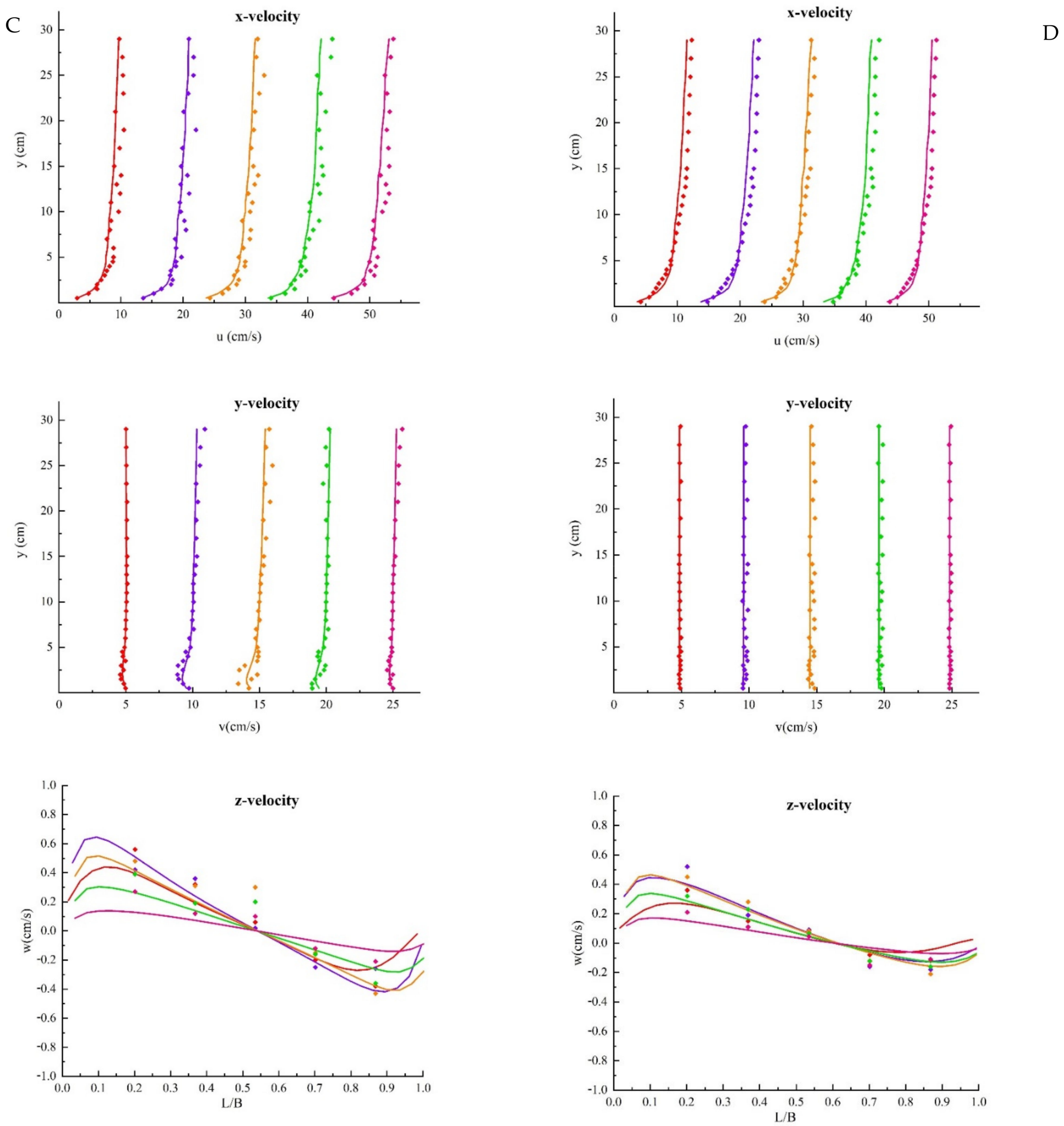

Figure 4. 3D velocity distribution and verification of each measured vertical line in Section S1–S4. (**A**) Section S1, (**B**) Section S2, (**C**) Section S3, (**D**) Section S4.

Table 1. Relative error of longitudinal velocity of each vertical line.

Section Number	Relative Error (%)									
	V1		V2		V3		V4		V5	
	Average	Maximum	Average	Maximum	Average	Maximum	Average	Maximum	Average	Maximum
S1	8.47%	19.96%	8.64%	14.83%	9.95%	15.24%	9.14%	15.75%	8.37%	14.92%
S2	7.49%	13.93%	4.88%	10.45%	6.56%	10.71%	5.51%	10.73%	4.81%	9.54%
S3	6.74%	13.96%	4.98%	14.30%	7.10%	14.33%	6.89%	14.04%	6.65%	13.84%
S4	6.59%	13.94%	7.23%	21.43%	5.67%	15.71%	7.79%	21.25%	6.32%	15.00%

3.2. 3D Flow Structure

The 3D flow velocity distributions of three typical horizontal sections were obtained, as shown in Figure 5.

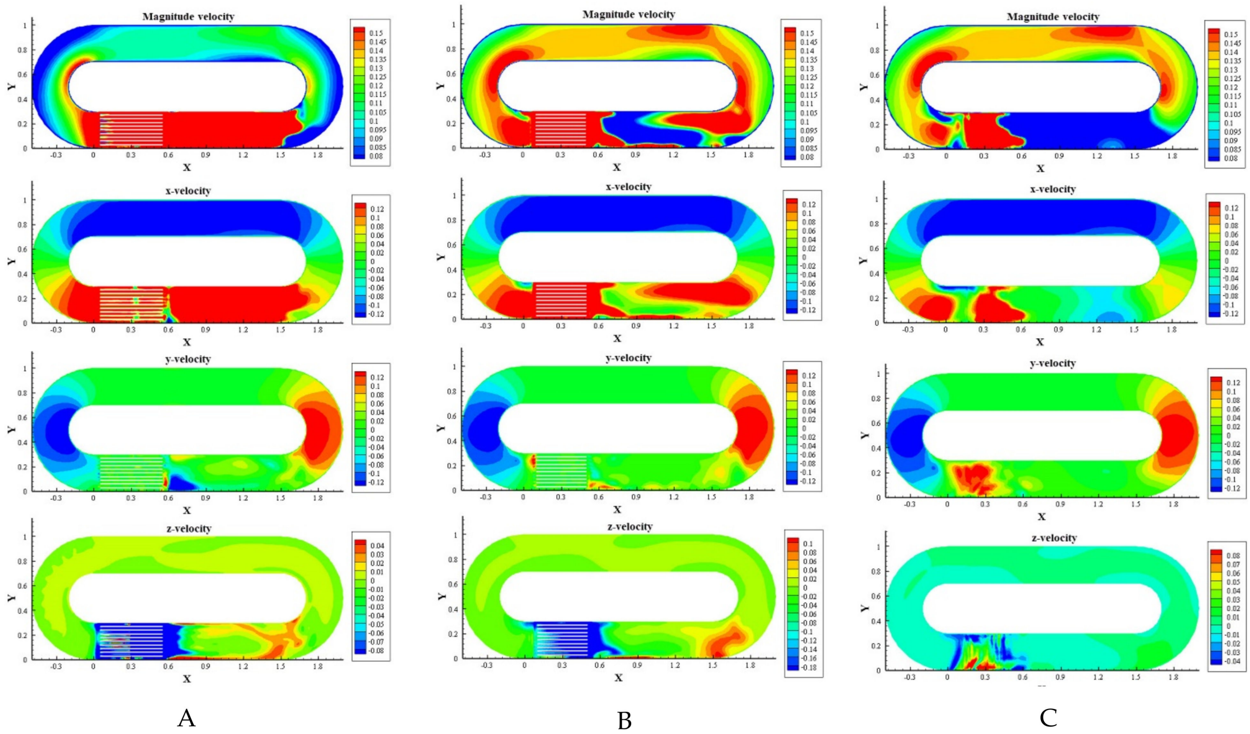

Figure 5. 3D velocity distribution at different elevations in flume. (**A**) z = 2 cm, (**B**) z = 15 cm, (**C**) z = 28 cm.

3.2.1. Straight I

The rotation of the wheel drives the water flow to the right, and this was the only power source of the water flow. The water flow around the rotary table was complex. On the left part of the wheel axis, the acting force was mainly reflected in the vertical direction, and the longitudinal driving force was very small. On the right part of the wheel axis, the acting force was more reflected in the longitudinal direct flow to the right of the movement. Beyond a distance of about 70 cm away from the wheel's axis, the wheel's influence gradually decreased. After a straight path, the flow field gradually tended towards stability. The longitudinal velocity showed a decreasing trend from the bottom to the water surface. The average velocity of the near surface layer was about 6.6–7.4 cm/s, with the middle layer being about 9.5–10.8 cm/s and the near bottom layer being about 12.3–13.5 cm/s.

3.2.2. Curve I

When the water enters curve I, the flow direction of the water is forcibly changed by the action of the side wall. The concave wall can change the direction of the water flow, with the inertia of the water flow impacting the concave wall. The concave wall exerted a counter-force on the water flow, forcing the water flow to turn along the wall, and the momentum change of the water flow caused the redistribution of water flow velocity. Under the action of inertial centrifugal force and radial pressure difference, the transverse velocity and vertical velocity combined to form a cross section circulation. The combination of the circulation and the longitudinal flow created a spiral flow, resulting in a spiral shape for the entire flow [23,24].

3.2.3. Straight II

The flow within 60 cm of the bending section was affected by the bending flow, and the flow velocity on the concave bank was greater than that on the convex bank. After a correction of about 60 cm, the flow rate tended to become stable and uniform, showing a state of high velocity upper and low velocity lower. The average velocity of the near surface layer was about 11.75–12.5 cm/s, while that of the middle layer was about 10.5–11.5 cm/s and the near bottom layer was about 7.5–8.5 cm/s.

3.2.4. Curve II

The flow in curve II was similar to that of curve I in structure. Under the action of inertial centrifugal force and radial pressure difference, the transverse velocity and vertical velocity combined to form a cross section circulation, when superimposed with longitudinal flow, the flow moved forward in a spiral shape. In addition, the water flow before exiting the corner was affected due to the role of the wheel.

3.3. Uniformity of Flow Velocity

During water conservancy science and environmental science research, it is necessary to perform experiments under stable, uniform conditions that are as close to the hydrodynamic characteristics of natural water as possible. Considering that curve I and II have obvious curve flow characteristics and straight I is affected by the wheel, the velocity uniformity of straight II was calculated. According to the calculation method for the velocity uniformity index in Section 2.8 of this paper, the uniformity of the 3D velocity along the path was calculated in straight II (see Figure 6).

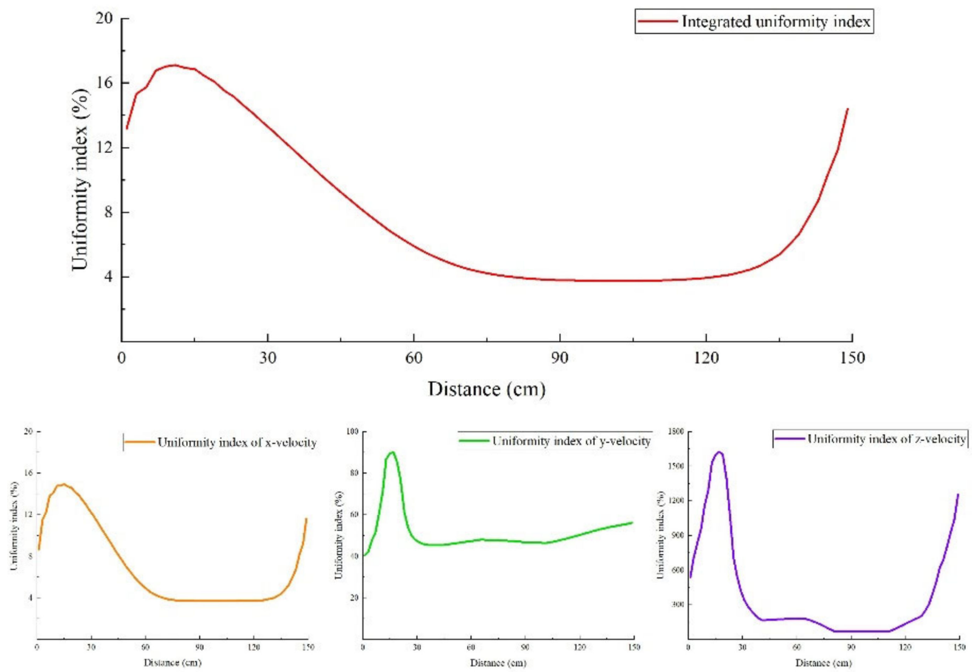

Figure 6. The distribution of 3D velocity uniformity along the path in straight II.

Figure 6 shows that as the distance of water in straight II increases, the velocity uniformity first deteriorates and then rapidly improves, and it did not get worse again until just before the curve. The uniform section of the flow field in the flume was not distributed symmetrically on both sides of the center of the straight path. It was closer to the back end of the straight. The uniformity of longitudinal velocity improved rapidly from 15.5% at 15 cm to 4% at 60 cm, and then remained basically stable until beginning to deteriorate rapidly at 135 cm. The uniformity of transverse and vertical velocity was similar to that of the longitudinal velocity along the longitudinal distance. The average transverse and vertical velocity was small; in particular, the average vertical velocity was close to 0, and the uniformity index was many orders of magnitude larger than that of the longitudinal velocity.

3.4. Influence of Rotational Speed on Velocity Uniformity

On the basis of the existing models, the wheel rotation speed was set at 20, 40, 60 and 80 rpm, respectively, for the numerical simulation. The uniformity distribution of the flow field at each rotational speed was obtained in straight II. It can be seen from Figure 7 where, taking the comprehensive uniformity coefficient 10% as the limiting condition, the corrected distances were 39, 71, 97 and 101 cm, respectively, and the corresponding uniform lengths were 106, 74, 50 and 46 cm. Corrected distance is positively correlated with rotational speed (average velocity), and the length of uniform section is negatively correlated with speed. Both of them have nonlinear correlation. This is because the increase in speed causes the fluid to collide more violently, leading to an increase in velocity inhomogeneity. When the speed is low, the correction distance and the length of uniform section change significantly with the increase in speed. When the speed reaches a certain degree, the influence of the increase of the speed on the correction distance and the length of uniform section is gradually weakened. In addition, the influence of outflow on velocity uniformity is much greater than that of inflow. The uniform section of the flow field in the flume is not distributed symmetrically on both sides of the center of the straight path. It is closer to the back end of the straight.

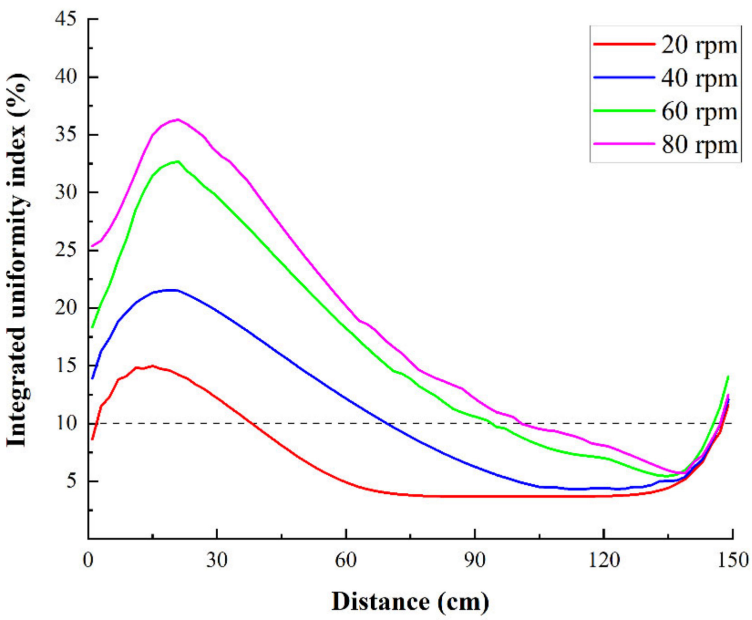

Figure 7. The distribution of velocity uniformity along the path at different speeds in straight II.

3.5. Similarity to Natural Gravity Flow Characteristics

3.5.1. Flow Structure

The motion of water in nature is caused by gravity, resistance and inertia forces. Gravity force generally dominates in straight section. Prandtl proposed in 1925 that the flow rate varies logarithmically with depth. In addition, velocity exponential distribution has been proposed. The distribution of time-averaged velocity on the cross section results in the surface velocity being large, while the bottom velocity is small. The longitudinal velocity generated by the device at each vertical line of section S3 in straight II was fitted with the Prandtl logarithmic distribution formula (see Formula (8)).

$$u = \frac{u_*}{\kappa}\ln z + C \quad (15)$$

where u is time average velocity, u_* is friction velocity, κ is Karman constant, z is distance from the bed surface, and C is integration constant.

In previous studies, the driving devices of circular flumes were located at the water surface or side wall. The larger part of the velocity gradient was also located near the water surface or side wall. According to the fitting results (see Table 2), different from previous research, the flow structure simulated by the flume in this paper was more in line with the gravity flow characteristics of a natural river.

Table 2. The longitudinal velocity fitting parameters with the Prandtl logarithmic distribution formula at section S3 of Straight II.

Vertical Number	$\frac{u_*}{\kappa}$	C	R^2
V1	$0.01706 \pm 6.77561 \times 10^{-4}$	0.13867 ± 0.00192	0.97895
V2	$0.01774 \pm 7.50101 \times 10^{-4}$	0.14544 ± 0.00213	0.97737
V3	$0.01660 \pm 6.57043 \times 10^{-4}$	0.13427 ± 0.00186	0.97894
V4	$0.01717 \pm 4.01164 \times 10^{-4}$	0.13185 ± 0.00114	0.97926
V5	$0.01540 \pm 6.00676 \times 10^{-4}$	0.12622 ± 0.00170	0.97992

3.5.2. Comparison with Natural Water Velocity

According to the Newton's Law of Similarity in Basic Principles of Hydraulic Similitude, the dynamic similarity of the two liquids under gravity means that their Froude Numbers (Fr) are the same. To be specific, the Froude number (Fr) under laboratory conditions is equal to that under field conditions.

$$\mathrm{Fr} = \frac{u}{\sqrt{gh}} \tag{16}$$

where Fr is the Froude Number, g is the gravitational acceleration, and h is the water depth.

According to the similarity principle above, the average velocity of the annular flume at a water depth of 0.3 m was converted into the average velocity of natural water under different water depth conditions, see Table 3.

Table 3. Conversion relation of equivalent average velocity at different water depths.

Water Depth (m)	0.3	1	3	10	20	30
Equivalent Velocity (m/s)	0.095	0.173	0.300	0.548	0.776	0.950

The results show that, when the water depth is 3 m, the equivalent velocity is 0.300 m/s, which is close to the average velocity of the plain river network area. When the water depth is 30 m, the equivalent velocity is 0.950 m/s, which is close to the average velocity of large rivers such as the Yangtze River. It follows that the depth of the experimental apparatus was relatively shallow, leading to the average velocity of flume being less than that of natural river in value. However, in terms of flow similarity, the device can basically cover the normal average velocity range of natural rivers and lakes.

4. Conclusions

In this study, a 3D mathematical model was established by using the commercial computational fluid dynamics (CFD) code Fluent software package to simulate its hydrodynamic characteristics. The accuracy of the mathematical model was further verified on the basis of the ADV measurement results. A new method was presented to calculate the distribution of the velocity uniformity coefficient in the straight section of the flume and quantify the uniformity index. The effect of rotational speed on velocity uniformity was studied. Finally, the similarity to natural gravity flow characteristics was discussed. The following results were obtained from the current study.

- ◆ The mathematical model established using the MRF model of the Fluent software was able to simulate the flow velocity distribution and flow field variation along each curve and straight path in the annular flume well.

- Straight II was less affected by the wheel, and the velocity uniformity was better in the middle segment after a long straight section of automatic correction. In particular, the comprehensive uniformity coefficient of 70–130 cm section was up to 5%, which proved that this section was a stable and uniform flow field zone.
- In the middle of Straight II, the longitudinal velocity conformed to the Prandtl logarithmic distribution, and the R^2 value was above 0.975. This was different from previous circular flumes, where the driving devices were located at the water surface or side wall. The flow structure of the device was more in line with the gravity flow characteristics of natural rivers. Furthermore, in terms of flow similarity, the device can basically cover the normal average velocity range of natural rivers and lakes.
- Corrected distance was positively correlated with rotational speed (average velocity), and the length of uniform section was negatively correlated with the speed. Both of them had a nonlinear correlation. The uniform section of the flow field in the flume was not distributed symmetrically on both sides of the center of the straight path. It was closer to the back end of the straight.
- This study can provide technical support for the research and development of different types of flume, exploration of water flow structure, and analysis of flow velocity uniformity. In addition, it can be used in related scientific research fields such as sediment, pollutant release, migration and diffusion.

Author Contributions: Conceptualization, L.H.; Formal analysis, Y.Z., B.C. and A.J.; Funding acquisition, L.H.; Investigation, L.H.; Methodology, Y.Z. and L.H.; Software, Y.Z., L.C., C.W. and B.C.; Supervision, L.C.; Writing—original draft, Y.Z. and C.W.; Writing—review & editing, Y.Z. All authors have read and agreed to the published version of the manuscript.

Funding: This research was funded by the National Natural Science Foundation of China (Grant No. 51979079). This research was in part supported by the Fundamental Research Funds for the Central Universities (Grant No. B200204033) and grants from a project funded by the Priority Academic Program Development (PAPD) of Jiangsu Higher Education Institutions.

Institutional Review Board Statement: Not applicable.

Informed Consent Statement: Not applicable.

Data Availability Statement: All data generated or analyzed during this study are included in this article.

Conflicts of Interest: The authors declare no conflict of interest.

References

1. Han, L.X.; Wai, W.H. Numerical simulation of flow characteristics in elongated annular flume. *J. Hohai Univ.* **2003**, *6*, 38–42.
2. Tang, H.W.; Zhao, H.Q.; Li, Z.W.; Yuan, S.Y.; Li, Q.X.; Ji, F.; Xiao, Y. Phosphorus sorption to suspended sediment in freshwater. *Water Manag.* **2016**, *170*, 231–242. [CrossRef]
3. Zheng, S.S.; Wang, P.F.; Wang, C.; Hou, J. Sediment resuspension under action of wind in Taihu Lake, China. *Int. J. Sediment Res.* **2015**, *30*, 48–62. [CrossRef]
4. Yang, Z.Q.; Baptista, A.; Darland, J. Numerical modeling of flow characteristics in a rotating annular flume. *Dyn. Atmos. Oceans.* **2000**, *31*, 271–294. [CrossRef]
5. Xin, G.Y.; Hu, C.C. Preventing eutrophication by using the hydrodynamic condition. *Yellow River.* **2006**, *7*, 36–37.
6. Wu, D.; Hua, Z.L. The effect of vegetation on sediment resuspension and phosphorus release under hydrodynamic disturbance in shallow lake. *Ecol. Eng.* **2014**, *69*, 55–62. [CrossRef]
7. Zheng, S.S.; Wang, P.F.; Wang, C.; Hou, J.; Qian, J. Distribution of metals in water and suspended particulate matter during resuspension processes of Taihu Lake sediment, China. *Quat. Int.* **2013**, *286*, 94–102. [CrossRef]
8. Vriend, H.J. *Flow Measurements in Cured Rectangular Channel: Part 2. Rough Bottom*; Delft University of Technology: Delft, The Netherlands, 1981; pp. 5–81.
9. Rui, D.F. Numerical Model for Circumfluence and Movement of Sediment in Continuous Meandering River. Master's Thesis, Sichuan University, Chengdu, China, 2005.
10. Feng, L.H. Study on Numerical Simulation for 3-D Flow in Channel Bend. Master's Thesis, Yangzhou University, Yangzhou, China, 2007.
11. Wang, W. *A Hydrograph-Based Prediction of Meander Migration*; Texas A&M University: College Station, TX, USA, 2006.

12. Ding, Y.Q.; Sun, L.M.; Qin, B.Q.; Wu, T.; Shen, X.; Wang, Y. Characteristics of sediment resuspension in Lake Taihu, China: A wave flume study. *J. Hydrol.* **2018**, *561*, 702–710. [CrossRef]
13. Xu, G.H.; Sun, Z.H.; Fang, W.Y.; Liu, J.J.; Xu, X.B.; Lv, C.X. Release of phosphorus from sediments under wave-induced liquefaction. *Water Res.* **2018**, *144*, 503–511. [CrossRef] [PubMed]
14. Gu, J.; Mao, X.D.; Kuang, C.P.; Hu, C.F.; Shan, Y.C. Study on characteristics of phosphorus release from estuarine bed sediments under intermittent wave disturbance. *Chin. J. Hydrodyn.* **2016**, *6*, 751–759.
15. Hua, Z.L.; Dan, W.; Kang, B.B. Flow Resistance and Velocity Structure in Shallow Lakes with Flexible Vegetation under Surface Shear Action. *Am. Soc. Civ. Eng.* **2013**, *6*, 612–620. [CrossRef]
16. Lu, Q.; Wang, X.D.; Guan, J.Z.; Wang, Z.Y. Verification of 3-D Numerical Model for Open-channel Flows Based on Fluent. *Sci. Technol. Eng.* **2012**, *32*, 103–106.
17. Zhao, L.X.; Zhu, B.J. Application of different turbulence model in hydrocyclone numerical simulation. *China Pet. Mach.* **2008**, *36*, 56–60.
18. Zhou, J.; Yan, W.P.; Shi, L.G.; Kong, F.Z. Study on numerical simulation of flow field uniformity in inlet section of SCR reacto. *Therm. Power Ucneration.* **2009**, *38*, 22–25.
19. Zhang, L.; Yan, Y.F.; Ran, J.Y.; Xiu, H.X. Numerical simulation of flow distribution uniformity in TWC and optimal design of catalyst in CNG vehicle. *J. Chem. Ind. Eng.* **2005**, *56*, 167–168.
20. Tao, H.G.; Chen, H.X.; Xie, J.L.; Shu, Z.H.; Hu, Y.X.; Lu, H. Flow uniformity index based on area-weighted and mass-weighted average velocity. *CIESC J.* **2010**, 122–126.
21. Li, J.S.; Rao, M.J. Evaluation Methods of Sprinkler Water Nonuniformity. *Trans. Chin. Soc. Agric. Eng.* **1999**, *15*, 78–82.
22. Han, W.T.; Wu, P.T.; Yang, Q.; Feng, H. Advances and comparisons of uniformity evaluation index of sprinkle irrigation. *Trans. Chin. Soc. Agric. Eng.* **2005**, *21*, 172–176.
23. Huang, S.L.; Jia, Y.F.; Chang, H.; Wang, S.Y. Three-dimensional numerical modeling of secondary flows in a wide curved channel. *J. Hydrodyn.* **2009**, *21*, 758–766. [CrossRef]
24. Li, Y.H.; Zhou, H.J. Three-dimensional numerical model for the meandering flow. *Chin. J. Hydrodyn.* **2004**, *19*, 856–864.